

# **Cucurbituril-Mediated Stacking Mode Conversion of Noncovalent Dimer**

Jie Wu, Yongxue Li, Teng Zhao, Shuangqi Song, Hengzhi Zhang, Xiufang Xu, Heng-Yi Zhang,\* and Yu Liu\*

The precise control of the spatial arrangement of organic photoconductive molecules plays an essential role in the fields of optoelectronics and bio-imaging. Herein, three rigid diphenylpyridine substituted toluene derivatives p-BPy, m-BPy, o-BPy with angles of 180, 120 and 60 degrees, are synthesized, respectively. The crystal structures reveal that both p-BPy and m-BPy are J-aggregate mode, and m-BPy stacks in an antiparallel manner, while p-BPy is in the isotropically parallel. 2D nuclear magnetic resonance (2D NMR) experiments demonstrate that p-BPy and m-BPy still are J-aggregate mode in aqueous solution, and o-BPy does not stack. Cucurbit[8]uril (CB[8]) can bind two p-BPy or m-BPy molecules expectedly in its cavity, and the former still is J-aggregate like in the solid state and aqueous solution with fluorescence emission peak red-shifts from 490 to 570 nm. Surprisingly, the stacking pattern of two m-BPy molecules in the CB[8] cavity changes from antiparallel to isotropic, resulting in excimer emission with a quantum yield increases significantly from 26.6% to 97.1%. This observation suggests that the cavity of CB[8] can mediate the stacking mode conversion of the noncovalent dimer m-BPy, and could be useful for the design of organic photoconductive molecules in the future.

#### 1. Introduction

Precise control of the spatial arrangement of organic photoconductive molecules is of particular importance<sup>[1–4]</sup> due to their application in optoelectronic semiconductors,<sup>[5,6]</sup> light-emitting diodes,<sup>[7]</sup> bio-imaging fields, probes,<sup>[8]</sup> etc. These organic photoconductive molecules always include aromatic groups, but most aromatic molecules have a tendency to aggregate due to various intermolecular interactions (e.g., electrostatic interactions).<sup>[9]</sup> Dimers should be the simplest system for precisely arranging molecules experimentally and theoretically.<sup>[10,11]</sup> On the one hand, dimers in which two molecules stack predominantly faceto-face with the blue-shifted absorption spectrum are generally

J. Wu, Y. Li, T. Zhao, S. Song, H. Zhang, X. Xu, H.-Y. Zhang, Y. Liu College of Chemistry

State Key Laboratory of Elemento-Organic Chemistry

Nankai University Tianjin 300071, P. R. China

E-mail: hyzhang@nankai.edu.cn; yuliu@nankai.edu.cn

The ORCID identification number(s) for the author(s) of this article can be found under https://doi.org/10.1002/adom.202501470

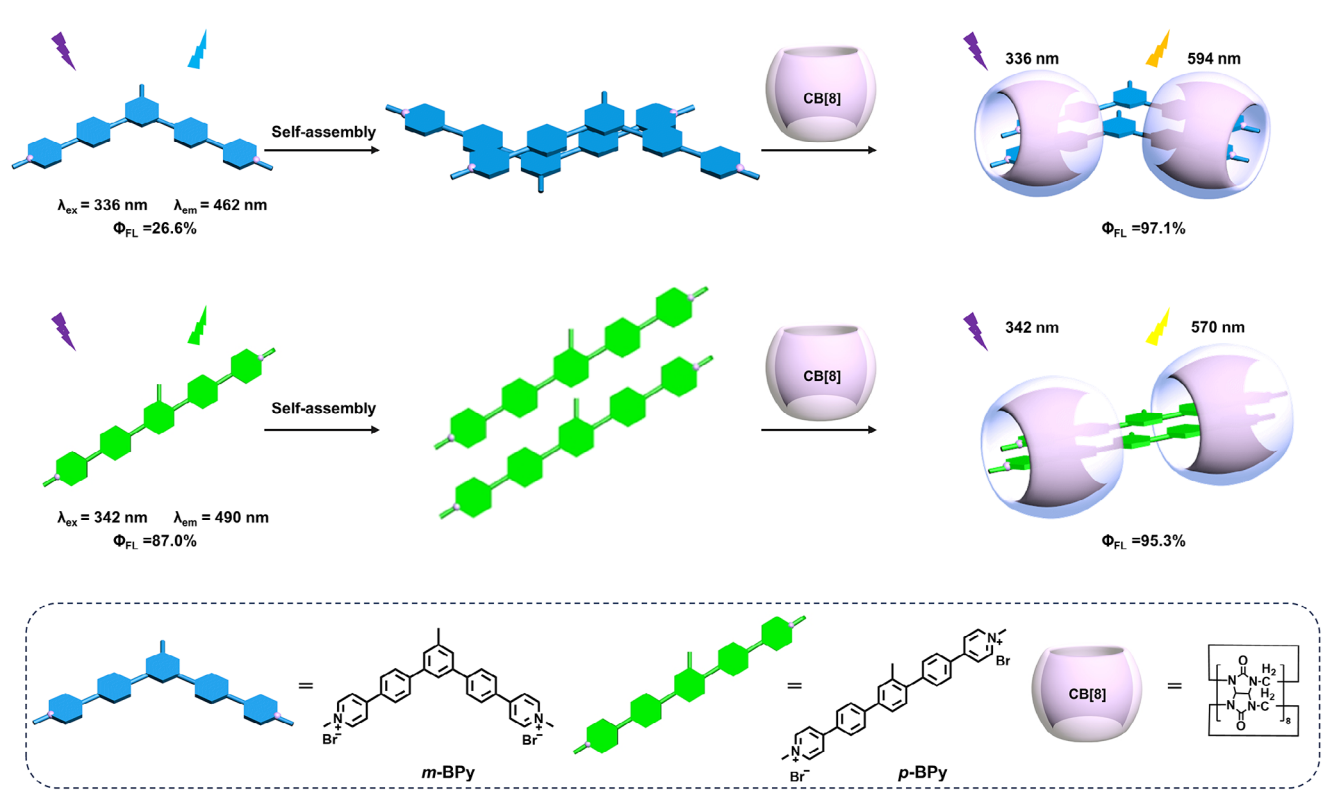
DOI: 10.1002/adom.202501470

named H-aggregates and exhibit low or no fluorescence mostly, and those in a head-to-tail arrangement with the red-shifted absorption spectrum are called J-aggregates. On the other hand, the formation of aggregates at high concentrations often results in two kinds of distinct fluorescent effects, namely "aggregation-caused quenching" (ACQ)<sup>[12]</sup> and "aggregation induced emission" (AIE).<sup>[13]</sup> A lot of research has been performed in both J-aggregates/H-aggregates of noncovalent dimers,<sup>[14-17]</sup> however, the effect of substituent orientation in the monomer molecule on photophysical performance was neglected.

Cucurbit[8]uril (CB[8]) can effectively bind two hetero-guests through host-stabilized charge-transfer interactions (HSCT)<sup>[18]</sup> and two homo-guests in its cavity and thus change the photophysical properties of guests. There have been many reports of the dimer between CB[8] and aryl pyridine derivatives.<sup>[19–24]</sup> For example, Scherman and co-workers used phenylpyridine molecules as rigid

"clamping" modules to build a series of fluorescent molecules that produce discrete dimer-stacked fluorophores when complexed with CB[8].[25] Another interesting example is the unexpectedly large molecular conductance of the pyridine dimer when it undergoes dimerization and  $\pi$ -stacking in the cavity of CB[8].[26] We were also interested in obtaining several homoguest dimers<sup>[27,28]</sup> and the molecular folding dimers<sup>[29–31]</sup> in the cavity of CB[8], and proved that a large Stokes shift of 367 nm and near-infrared emission, [27] the phototunable conversion from fluorescence to phosphorescence in aqueous media and dual organelle-targeted imaging, [28] and afterglow with high phosphorescence quantum yield over 99%.[30] Herein, we designed and synthesized three rigid molecules p-BPy, m-BPy, and o-BPy with an angle of 180, 120, and 60 degrees, respectively, and introduced a methyl to the rigid molecules in order to distinguish the stacking mode of noncovalent dimers of BPys. Using ultraviolet visible spectroscopy, fluorescence, nuclear magnetic resonance (NMR) spectra, isothermal titration calorimetry (ITC) and X-ray crystallography, we will show that the stacking mode of *p*-BPy always is J-aggregates both in the solid state and in aqueous solution of the presence and absence of CB[8], while m-BPy adopts two distinct aggregate modes in the presence and absence of CB[8] (Scheme 1).

21951011, 2025, 29, Downloaded from http://advanced on inlithelbrary.wile.com/doi/10.1002/adom. 202501470 by Nanki University, Wiley Online Library on [2610/2025]. See the Terms and Conditions (https://onlinelibrary.wiley.com/terms-and-conditions) on Wiley Online Library for less of use; OA articles as governed by the applicable Certains Commons



**Scheme 1.** Schematic illustration of CB[8] assembled with m-BPy and p-BPy.

# 2. Crystal Structure and Stacking Patterns of Noncovalent Dimers

The compounds p-BPy, m-BPy, and o-BPy were synthesized by Suzuki reaction of 1,4-dibromo-2-methyl-benzene, 1,3-dibromo-5-methylbenzene, and 1,2-dibromo-4-methylbenzene with 4-(pyridine-4-yl) phenylboronic acid, respectively, and followed Nmethylation with iodomethane and ion exchange (Scheme S1 and Figures S1-S14, Supporting Information). Their positive charge at the end can increase the water solubility and is beneficial to the complexation with cucurbituril in aqueous solution.<sup>[30]</sup> Light yellow acicular crystals of m-BPy and p-BPy were obtained by using the slow diffusion method, with hexafluorophosphate as the counterion (Table S3, Supporting Information, contains all crystal data). The crystal structure reveals that *m*-BPy conformation is distorted (Figure 1a,d), and two molecules are stacked in a reverse parallel manner via  $\pi$ - $\pi$  stacking interactions to form a pair of noncovalent dimers (Figure S15, Supporting Information). Its two methyl groups on the central benzene ring orientate in the opposite direction (Figure 1b,d). The slip angles and center distances between the two parallel benzene ring planes are 30.12°, 15.67°, and 4.009 Å, 3.705 Å, respectively (Figure 1c). In contrast, the p-BPy molecular conformation is relatively planar, with molecules stacked parallel to each other but offset by a distance equivalent to the size of a pyridine ring due to repulsion between the positive charges (Figure 1e,f and Figure S16, Supporting Information). And the center distances and slip angles between the two parallel rings in two adjacent p-BPy molecules are 3.87 Å, 3.97 Å, 4.00 Å, 3.93 Å and 23.7°, 17.82°, 26.51°, 24.18°, respectively (Figure 1f). Next, we investigated the stacking patterns of the three guests in aqueous solutions. These correlation peaks of b and c, b and d, d and e in 2D rotating-frame Overhauser effect spectroscopy (2D ROESY) of m-BPy (Figure S17, Supporting Information) demonstrate that two m-BPy molecules are stacked in a partially overlapping and antiparallel manner, which is the same as the stacking pattern of its crystal. The correlation peaks of b and c, b and  $d_2$ , e and  $d_1$  of p-BPy reveal that there exists a similar stacking mode in its aqueous solution as in its single crystal (Figure S18, Supporting Information). These results demonstrate that p-BPy and m-BPy molecules form J-aggregates in both the crystalline state and aqueous solution. However, there are no relevant peaks in Figure S19 (Supporting Information), suggesting that no noncovalent dimers are formed between two o-BPy molecules in aqueous solution.

## 3. The Photophysical Properties of BPys

The aqueous solution of *m*-BPy emits weak blue fluorescence at 462 nm, while the aqueous solutions of *p*-BPy (490 nm) and *o*-BPy (488 nm) at the same concentration exhibit bright green fluorescence under illumination by a 365 nm UV lamp, respectively. The maximum UV absorption peaks of *m*-BPy, *p*-BPy, and *o*-BPy are located at 332, 340, and 318 nm, respectively (Figure S20, Supporting Information). The fluorescence quantum yields of *m*-BPy, *p*-BPy, and *o*-BPy are 26.6%, 87.0% and 88.8%, respectively, with *m*-BPy showing the weakest emission brightness (13.94) among them (Figure S21 and Table S1, Supporting Information). We speculate that the energy of *m*-BPy may be dissipated through non-radiative pathways such as intramolecular vibration and rotation, rather than in radiative form. And the rotations of

21951071, 2025, 29, Downloaded from https

library.wiley.com/doi/10.1002/adom.202501470 by Nankai University. Wiley Online Library on [26/10/2025]. See the Terms and Conditions (https://onlinelibrary.wiley.com/terms-and-conditions) on Wiley Online Library for rules of use; O, A articles are governed by the applicable Creative Commons I

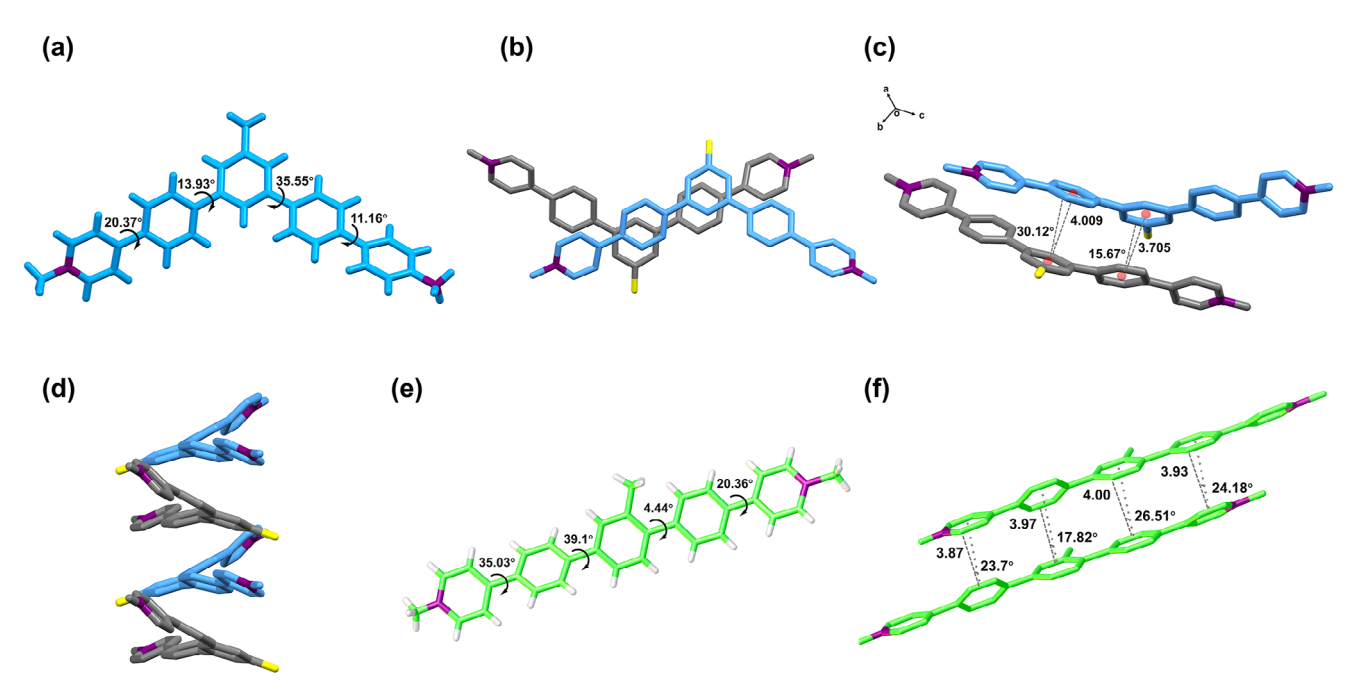


**Figure 1.** Crystal structures of a) *m*-BPy and e) *p*-BPy, with their conformations illustrated using dihedral angles. b) Self-assembly pattern of *m*-BPy (viewed along the b-axis). Methyl group is shown in yellow to reflect the relative position and orientation. Center distances and slip angles between parallel planes of adjacent molecule for c) *m*-BPy and f) *p*-BPy. d) The self-assembly modes of *m*-BPy (view along c-axis).

 $p ext{-BPy}$  and  $o ext{-BPy}$  are restricted by steric hindrance from the metamethyl and ortho-phenylpyridine groups, respectively. Glycerol, a viscous substance, can effectively impede molecular motion. To test this hypothesis, a series of glycerol-water mixtures were configured. As the ratio of glycerol increases, the fluorescence intensity of  $p ext{-BPy}$ ,  $m ext{-BPy}$  and  $o ext{-BPy}$  increases, with the largest enhancement observed for  $m ext{-BPy}$  (Figure S22, Supporting Information). These results support the above hypothesis and are further strongly corroborated by the higher non-radiative decay rate ( $K_{nr}$ ) of  $m ext{-BPy}$  and the higher of radiative decay rate ( $K_r$ ) of  $p ext{-BPy}$  and  $o ext{-BPy}$  (Table S1, Supporting Information). And we can conclude that  $m ext{-BPy}$  is easier to rotate compared to  $p ext{-BPy}$  and  $o ext{-BPy}$  in the aqueous solution.

# 4. Photophysical Properties of BPys Assembly with Cucurbituril

Macrocyclic cucurbituril was introduced into the aqueous solution of three guests to regulate the spatial arrangement. First of all, the stoichiometry of *m*-BPy⊂CB[8] is determined to be 1:1 according to the Job's plot (Figure S25a, Supporting Information). This complex is stable with a binding constant of 8.21 × 10<sup>5</sup> M<sup>-1</sup> in water at 298 K (Figure 2a). Next, UV and fluorescence spectra were measured to explore the photophysical behavior of *m*-BPy upon the continuous addition of CB[8] into its aqueous solution. With the addition of 1.8 equivalents of CB[8], the maximum UV absorption peak red shifts from 332 to 362 nm, and the absorbance decreases. Upon further addition of CB[8] up to 4.4 equivalents, the maximum UV absorption peak continues to red shift to 374 nm (Figure 2a). Enhanced blue fluorescence emission is observed from the fluorescence spectrum when CB[8] is added to 0.8 equivalents (Figure S25b, Supporting Informa-

tion). With further addition of CB[8] from 0.8 to 4.4 equivalents, the fluorescence intensity at 462 nm gradually diminishes and a new fluorescence peak appears at 594 nm (Figure 2b and Figure S25b,c, Supporting Information). The large Stokes shift of 220 nm indicates that two m-BPy molecules stack in the cavity of CB[8], resulting in excimer emission.[32,33] Excimer emission indicates the ratio between *m*-BPy and CB[8] is 2:2, rather than 1:1. When irradiated under a 365 nm handheld UV lamp, the addition of 1.8 and 2.0 equivalents of CB[8] result in white fluorescence and turn to orange upon further addition of CB[8] (Figure 2b). This phenomenon is illustrated by the 1931 CIE chromaticity diagram (Figure 2c). And the corresponding coordinates of white light emission of m-BPy $\subset 1.8$ eq CB[8] and m-BPy $\subset 2.0$ eq CB[8] are (0.30, 0.30) and (0.33, 0.32). These values are very close to the standard emission coordinates for pure white light, which are (0.33, 0.33). And the fluorescence spectra of them exhibit two fluorescence peaks (462 nm and 594 nm), covering the entire visible wavelength range from 400 to 700 nm.[38] White light emission requires either the simultaneous emission of red, green and blue or at least two complementary colours.[34-37] Herein, white light emission arises from a balance of two complementary colors: blue light (discrete guest) and orange ( $[m-BPy]_2 \subset CB[8]_2$ ). [38]

The p-BPy $\subset$ CB[8] complex is formed in a 1:1 stoichiometry, with a binding constant of  $1.768 \times 10^7$  M $^{-1}$  (Figure S26a, Supporting Information and Figure 2d). As shown in Figure S49, Supporting Information, the calculated binding energy of B2-CB[8] is 2.8 kcal/mol more negative than that of A2-C-CB[8], indicating the interaction between p-BPy and CB[8] is stronger than that between m-BPy and CB[8]. As a result, the binding constant of p-BPy is significantly higher than that of m-BPy. Although both p-BPy $\subset$ CB[8] and m-BPy $\subset$ CB[8] exhibit a 1:1 binding ratio, their UV and fluorescence spectra show significant differences. Upon

21951071, 2025, 29, Downloaded from https

elibrary.wiley.com/doi/10.1002/adom.202501470 by Nankai University, Wiley Online Library on [2610/2025]. See the Terms and Conditions (https://onlinebibrary.wiley.com/terms-and-conditions) on Wiley Online Library for rules of use; O.A articles are governed by the applicable Creative Commons

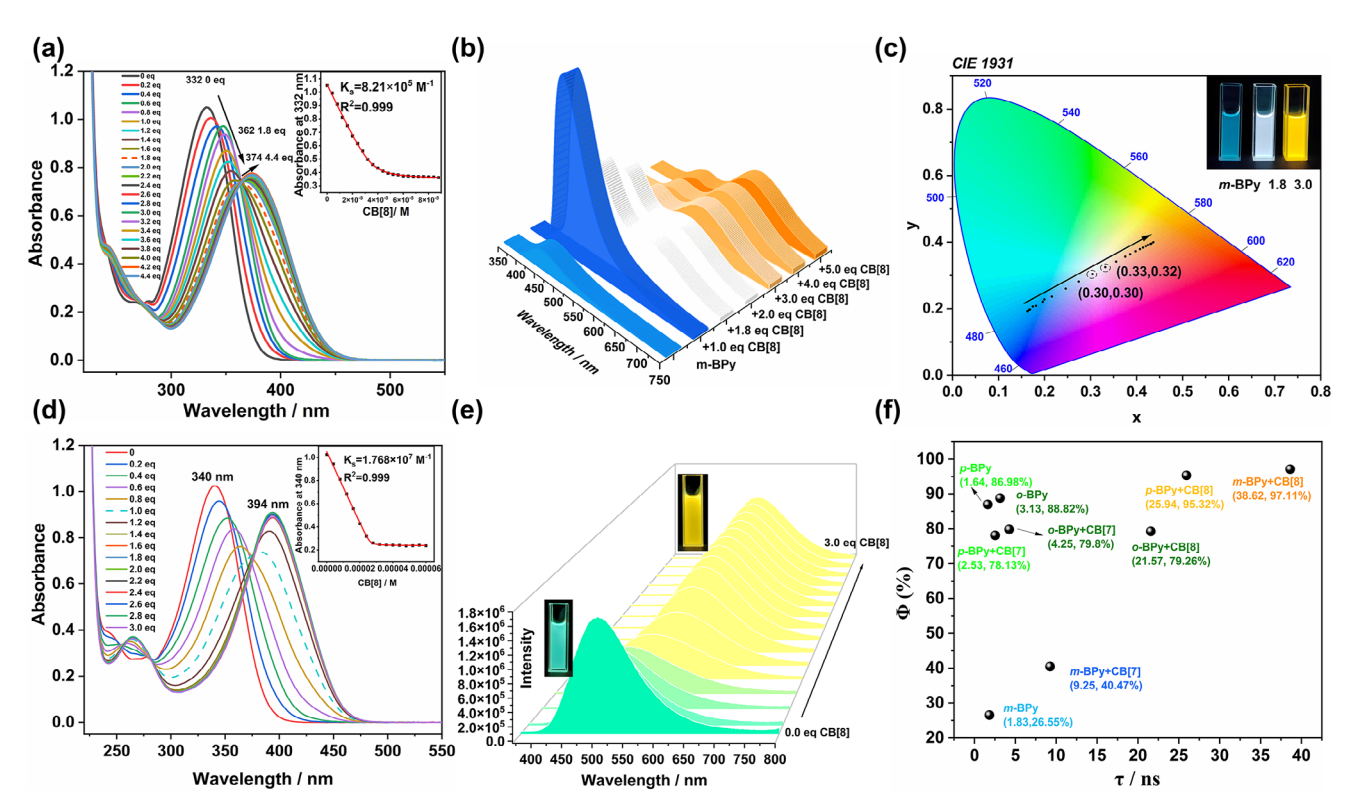


Figure 2. a) UV–vis absorption spectra of m-BPy in water upon the gradual addition of CB[8] at 298 K. The insert of (a) shows the  $K_S$  value between m-BPy and CB[8]. b) Fluorescence spectrum of m-BPy aqueous solution with the addition of 0–5.0 equivalents of CB[8]. c) Chromaticity coordinate (CIE) of m-BPy with different CB[8] ratios in H<sub>2</sub>O at 298 K. Inset: photographs of m-BPy solutions with 0.0 (left), 1.8 (middle) and 3.0 (right) equivalents of CB[8]. d) UV–vis absorption spectra of p-BPy in water upon the gradual addition of CB[8] at 298K. The insert of (d) shows the  $K_S$  value between p-BPy and CB[8]. e) Fluorescence spectra of p-BPy aqueous solution upon the addition 0–3.0 equivalents of CB[8]. f) Corresponding quantum yield (Φ) and lifetime ( $\tau$ ).

the addition of CB[8] from 0 to 3.0 equivalents, the UV absorption peak red shifts from 340 nm to 394 nm, accompanied by an initial decrease followed by an increase in absorbance (Figure 2d). Fluorescence titration experiments reveals that the fluorescence peak red shifts from 498 to 570 nm, with the fluorescence intensity initially decreasing and then increasing, while the color changes from green to yellow (Figure 2e and Figure S26b, Supporting Information).

Next, we explored the bonding modes and photophysical properties of m-BPy and p-BPy with CB[7], which has a smaller cavity than CB[8]. First, both m-BPy and p-BPy form 1:2 complexes with CB[7] (Figures S27a and S28a, Supporting Information), with bonding constants of  $6.53 \times 10^{12} \text{ M}^{-2}$  and  $6.7 \times 10^{10} \text{ M}^{-2}$ in water at 298 K, respectively (Figures S27c and S28c, Supporting Information). Subsequently, diffusion coefficients (D) of m-BPy, m-BPy⊂CB[8], and m-BPy⊂CB[7] were determined to be  $3.192 \times 10^{-10}$ ,  $2.046 \times 10^{-10}$ , and  $2.159 \times 10^{-10}$  m<sup>2</sup> s<sup>-1</sup> in the diffusion ordered spectroscopy (DOSY) experiments (Figure S29, Supporting Information). The diffusion coefficients (D) of p-BPy, p-BPy $\subset$ CB[8], p-BPy $\subset$ CB[7] are  $3.503 \times 10^{-10}$ ,  $1.727 \times 10^{-10}$ ,  $2.046 \times 10^{-10} \text{ m}^2 \text{ s}^{-1}$  (Figure S30, Supporting Information). As is well known, a larger diffusion coefficient indicates a smaller diameter of the formed nanoparticles. The diffusion coefficients of m-BPy $\subset$ CB[7] and p-BPy $\subset$ CB[7] are larger than those of m-BPy $\subset$ CB[8] and p-BPy $\subset$ CB[8], indicating that the particle sizes of *m*-BPy⊂CB[8] and *p*-BPy⊂CB[8] are larger. This further illustrates that m-BPy and p-BPy formed 2:2 quaternary complexes with CB[8] and 1:2 ternary complexes with CB[7]. And the significant redshift in their emission spectra indicates that m-BPv and p-BPy molecules have formed J-aggregates in the CB[8] cavity, respectively. Upon the continuous addition of CB[7], the maximum UV absorption peak of m-BPy red shifts from 332 nm to 344 nm, accompanied by a decrease in absorbance (Figure S27b, Supporting Information). The fluorescence intensity continues to increase while maintaining blue fluorescence, as CB[7] restricts the movement of m-BPy (Figure S27d, Supporting Information). A similar phenomenon is observed upon the continuous addition of CB[7] to p-BPy aqueous solution (Figure S28, Supporting Information). The quantum yields and lifetimes of m-BPy and p-BPy increase significantly upon complexation with CB[8]. The quantum yield increases from 26.6% to 97.1% for m-BPy and 87.0% to 95.3% for p-BPy (Figures S21 and S31, Supporting Information and Figure 2f). As shown in Figure S48 (Supporting Information), A2-C is 8.1 kcal mol<sup>-1</sup> lower in energy than A2, indicating the configuration of A2-C is more stable than A2. The enhanced stability of A2-C can be attributed to stronger  $\pi$ – $\pi$  interactions between the two *m*-BPy molecules. And the stronger  $\pi$ – $\pi$  interactions effectively prevent the rotation of certain C–C single bonds in A2-C at the excited state, and thereby suppress nonradiative energy dissipation. As a result, higher fluorescence quantum yield

www.advancedsciencenews.com

21951071, 2025, 29, Downloaded from https

Hibrary.wiley.com/doi/10.1002/adom.202501470 by Nankai University, Wiley Online Library on [26/10/2025]. See the Terms and Conditions (https://onlinelibrary.wiley.com/terms

conditions) on Wiley Online Library for rules of use; OA articles are governed by the applicable Creative Commons

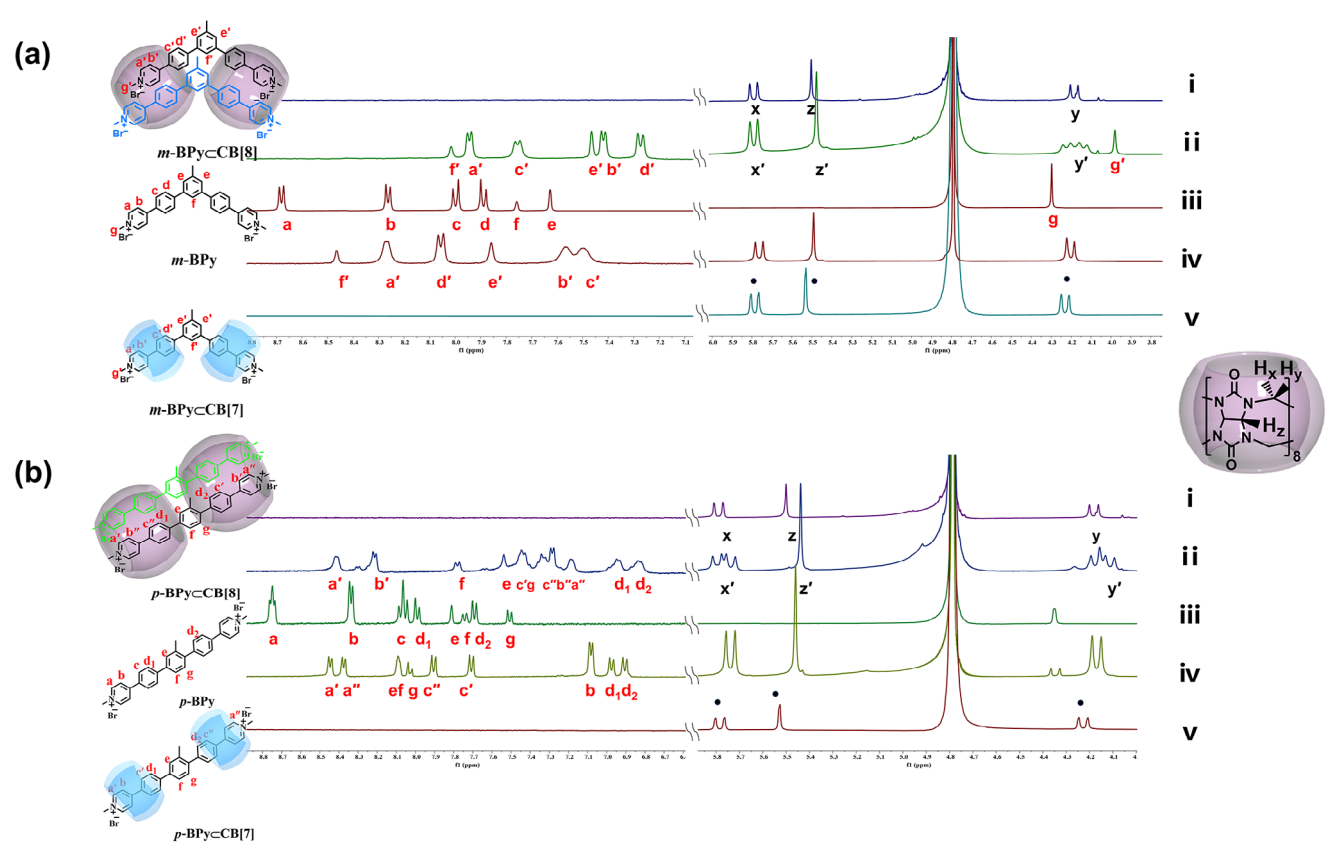


Figure 3. ¹H NMR spectra of a)i) CB[8], ii) m-BPy⊂CB[8], iii) m-BPy, iv) m-BPy, cb[7], v) CB[7], b)i) CB[8], ii) p-BPy⊂CB[8], iii) p-BPy, iv) p-BPy⊂CB[7], v) CB[7] ([m-BPy] = [p-BPy] = 1 mm, CB[7] = CB[8] = 2 mm, 400 MHz,  $D_2O$ ). The CB[7] protons are labeled as ( $\bullet$ ).

is observed for A2-C, which is consistent with the experimental results. And the lifetime increases from 1.83 to 38.62 ns for m-BPy and 1.64 ns to 25.94 ns for p-BPy (Figures S32 and S33, Supporting Information). The quantum yields and lifetimes of m-BPy and p-BPy after encapsulation with CB[8] are much larger than those encapsulated with CB[7]. The quantum yield of m-BPyCCB[8] is twice that of m-BPyCCB[7]. Fluorescence and UV spectra indicate that the interactions between o-BPy and CB[7] or CB[8] are very weak due to steric hindrance (Figure \$34, Supporting Information). Since the cavity of CB[7] is smaller than that of CB[8], CB[7] is bonded to the pyridine portion of o-BPy, while CB[8] is bonded to the phenylpyridine portion (Figures \$35 and S36, Supporting Information). And o-BPy does not accumulate in aqueous solution, so the next section does not discuss o-BPy.

## 5. Evidence of [BPys]<sub>2</sub> ⊂CB[8]<sub>2</sub> from <sup>1</sup>H NMR

Subsequently, <sup>1</sup>H NMR experiments were conducted to determine the binding sites of m-BPy and p-BPy with CB[7] and CB[8], respectively. The four groups of aromatic hydrogen (H-a, H-b, Hc, H-d) on the phenyl and pyridine and the H-e on the benzene ring of *m*-BPy⊂CB[8] upfield shift ( $\Delta \delta$  = -0.74, -0.84, -0.24, -0.62, -0.16 for H-a, H-b, H-c, H-d and H-e, respectively), which indicates that two phenyl pyridines are encapsulated in the CB[8] cavity. The methyl H-g on the nitrogen atom of the pyridine ring also upfield shift ( $\Delta \delta$  = -0.32), suggesting an inclusion near the CB[8] portal or it is an average signals generated by a partial inclusion

and partial exclusion by the cavity. [39] The H-f on the intermediate benzene ring downfield shift ( $\Delta \delta = 0.26$ ), indicating it near the port of CB[8] (Figure 3a).[39] However, the protons H-a, H-b and H-c of the phenyl and pyridyl groups of *p*-BPy⊂CB[8] exhibit two sets of signals (Figure 3b). And the upfield shifts of H-a, Hb, H-c, H-d<sub>1</sub>, H-d<sub>2</sub>, H-e, H-g, suggesting that the bonding site remains at the phenylpyridine moiety. Furthermore, the CB[8] proton H<sub>v</sub> (located outside the cavity) and H<sub>v</sub> (located inside the cavity) of p-BPyCCB[8] split into two sets of peaks, revealing that portal of CB[8] is always exposed to a more positive charge than the other, forming an asymmetric environment.[39] The bonding sites of *p*-BPy⊂CB[7] is also identified as the phenylpyridine moiety (Figure 3). The aromatic hydrogen (H-a, H-b, H-c) on the phenyl and pyridine ring of *m*-BPy⊂CB[7] upfield shift, but the H-d downfield shift. This proves that the bonding site of m-BPyCCB[7] is the pyridine ring (Figure 3, Figures S37 and S38, Supporting Information).

The ¹H NMR titration of *m*-BPy⊂CB[8] shows that an equilibrium reaches at 0.5 equivalents upon the addition of CB[8], followed by another equilibrium at 1.0 equivalents (Figure \$39, Supporting Information). In addition, the two peaks on pyridine split into two sets of signals: one shifts downfield indicating interaction with CB[8], and the other remains at the original position (free m-BPy). This observation suggests that the association and dissociation of *m*-BPy and *m*-BPy⊂CB[8] complexes undergo slow exchange on the <sup>1</sup>H NMR time scale (Figure \$39, Supporting Information). The ITC curve also reveals two equilibria,

21951071, 2025, 29, Downoloaded from https://advanced.onlinelibrary.wiley.com/doi/10.1002/adom.20250147 by Nankai University. Wiley Online Library on [26/10/2025]. See the Terms and Conditions (https://onlinelibrary.wiley.com/terms-and-conditions) on Wiley Online Library for rules of use; OA articles are governed by the applicable Creative Commons Licensenses.

www.advopticalmat.de

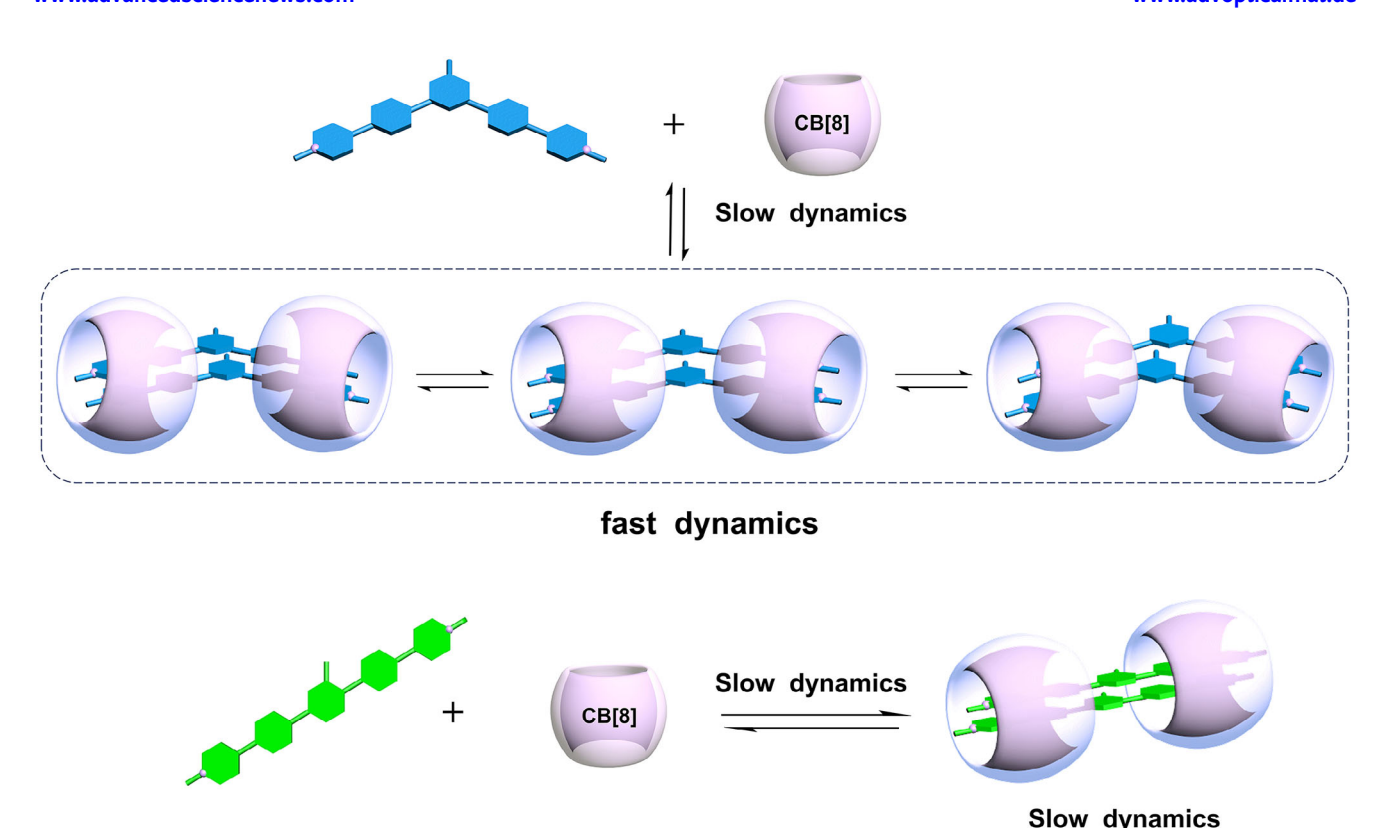


Figure 4. Two dynamic processes involved in the 2:2 quaternary host-guest complex.

indicating a transition from a 1:2 (m-BPy: CB[8]) to a 2:2 bonding mode (Figure S40, Supporting Information). In contrast, the association and dissociation of m-BPy and m-BPy $\subset$ CB[7] complexes undergo fast exchange on the  $^1$ H NMR time scale (Figure S41, Supporting Information). Besides, the  $^1$ H NMR titration profile of p-BPy $\subset$ CB[8] reveals that the association and dissociation of both p-BPy and p-BPy $\subset$ CB[8] complexes also undergo slow exchange on the  $^1$ H NMR time scale (Figure S42, Supporting Information).

The ¹H spectra of *m*-BPy⊂CB[8] and *p*-BPy⊂CB[8] are quite different. Only one set of signals is observed for the phenyl and pyridyl protons of *m*-BPy⊂CB[8]. This phenomenon may be attributed to the rapid oscillation of the two *m*-BPy guests within the CB[8] cavity, accompanied by fast interconversion between different overlapping conformations. However, *p*-BPy⊂CB[8] shows two sets of signals for all protons of the phenyl and pyridyl groups, indicating a slower internal transition. And both *m*-BPy⊂CB[8] and *p*-BPy⊂CB[8] exhibit slow intermolecular bonding and dissociation according to the ¹H NMR titration results. These observations demonstrate the existence of two distinct kinetic processes in the 2:2 quaternary complexes (**Figure 4**).<sup>[39]</sup>

# 6. Evidence of [BPys]<sub>2</sub> ⊂CB[8]<sub>2</sub> from 2D NMR

Then, we determined the relative spatial position of the two m-BPy molecules within the cavity of CB[8]. First, we used COSY (chemical shift correlation spectroscopy) spectroscopy to assign the proton signals (Figure S43, Supporting Information). The ROESY spectrum of m-BPy $\subset$ CB[8] displays that the methyl H-

g' of the pyridine nitrogen atom correlates with H-a' and H-b' on the pyridine. And H-c' on the benzene ring is correlated with H-f', H-e' on the middle benzene ring and central methyl group H-h' (Figure \$44, Supporting Information). These correlation signals indicate the two m-BPy molecules are J-aggregated in the cavity of CB[8]. It also confirms that m-BPy and CB[8] form a 2:2 head-to-head overlapping host-guest complex, as illustrated in Figure 5.[40] Notably, the methyl groups on the central benzene rings of the two encapsulated m-BPy molecules are oriented in the same direction, which is significantly different from the stacking pattern observed in aqueous solution. This demonstrates that CB[8] transforms the stacking arrangement of the noncovalent m-BPy dimer from an antiparallel to an isotropic parallel arrangement. Numerous studies have reported the importance of size complementarity, hydrophobic effects (entropic gain from water release upon binding) and direct host-guest interactions in the complexation of CB[n] with guests. [41–43] For example,

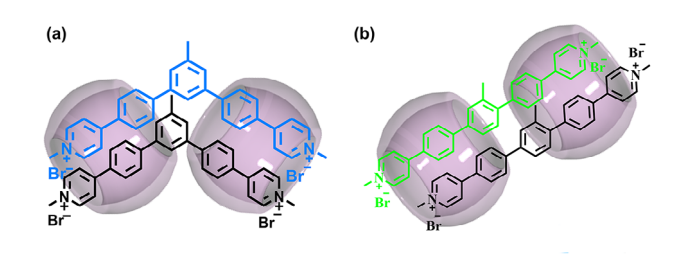


**Figure 5.** Bonding patterns between *m*-BPy, *p*-BPy and CB[8], respectively.

ADVANCED
OPTICAL
MATERIALS

21951071, 2025, 29, Downloaded from https

elibrary.wiley.com/doi/10.1002/adom.202501470 by Nankai University, Wiley Online Library on [26/10/2025]. See the Terms and Conditions

and-conditions) on Wiley Online Library for rules of use; OA articles are governed by the applicable Creative Commons

Frank Biedermann reports that the release of "high-energy" cavity water molecules into the bulk aqueous phase provides a strong enthalpic driving force for association, which is directly related to the number of water molecules displaced. [44–46] Based on this, we propose that the release of high-energy cavity water may provide a strong enthalpic driving force for the bonding of CB[8] to *m*-BPy and induce a 180° rotation of another *m*-BPy molecule.

We first employed COSY spectroscopy to assign the proton signals of *p*-BPy⊂CB[8] (Figure S45, Supporting Information). The ROESY spectrum displays cross-peaks a"-d2 and b"-d1 between the benzene and pyridine rings, inferring that the two p-BPy molecules maintain a J-aggregate mode and also form a 2:2 headto-head host-guest complex with CB[8] (Figure S46, Supporting Information and Figure 5). And TEM images reveal that both m-BPy and *p*-BPy are nanospheres, *m*-BPy⊂CB[8] and *p*-BPy⊂CB[8] are nanosheet, which further prove that m-BPy and p-BPy all form 2:2 head to head host guest complex with CB[8] (Figure S47, Supporting Information). The result demonstrates that p-BPy molecules are consistently J-aggregates both in the presence and absence of CB[8] in aqueous solution. Therefore, CB[8] converts the stacking pattern of *m*-BPy from antiparallel to isoparallel, while maintaining the original J-aggregate stacking mode of p-BPy.

#### 7. Conclusion

We synthesized three cationic guests *m*-BPy, *p*-BPy and *o*-BPy by simply changing the substitution position of one phenylpyridine. Notably, the crystal structures demonstrate that m-BPy molecules are stacked in an anti-parallel manner, while the p-BPy molecules are stacked isotropically parallel. In addition, 2D NMR results reveal that CB[8] can induce a transition of noncovalent m-BPy dimer from antiparallel to isotropic parallel. However, it does not affect the stacking pattern of p-BPy. The p-BPy molecules always are J-aggregates both in aqueous solution of the presence and absence of CB[8]. Besides, <sup>1</sup>H NMR experiments demonstrate that the intermolecular binding and dissociation of [*m*-BPy]<sub>2</sub> ⊂CB[8]<sub>2</sub> and [p-BPy]₂ CB[8]₂ is slow, but intra-conversion processes are faster for m-BPy but slower for p-BPy. Remarkably, the orientation of the substituents in the monomer molecule has a great influence on the photophysical properties. [*m*-BPy]<sub>2</sub> ⊂CB[8]<sub>2</sub> exhibits excimer emission with fluorescence peaks at 462 and 594 nm. The fluorescence spectrum of [p-BPy], CCB[8], shows only a single peak at 570 nm. And we achieve tunable multicolor fluorescence including blue, white, orange, green, and yellow emission by modulating the ratio of CB[8] and single guest in aqueous solution. This approach may be applied to the design of organic photoconductive molecules in the future.

#### Supporting Information

Supporting Information is available from the Wiley Online Library or from the author.

### Acknowledgements

This work was financially supported by the National Natural Science Foundation of China (22271165) and the Fundamental Research Funds for the Central Universities, Nankai University.

#### **Conflict of Interest**

The authors declare no conflict of interest.

#### **Data Availability Statement**

The data that support the findings of this study are available from the corresponding author upon reasonable request.

#### Keywords

cucurbituril, dimers, host–guest interaction, phenylpyridine derivatives, photophysical behavior

Received: May 8, 2025 Revised: July 31, 2025 Published online: August 26, 2025

- [1] G. L. Wu, F. Li, B. H. Tang, X. Zhang, J. Am. Chem. Soc. 2022, 144, 14962
- [2] M. Olesińska, G. L. Wu, S. Gómez-Coca, D. Antón-García, I. Szabó, E. Rosta, O. A. Scherman, Chem. Sci. 2019, 10, 8806.
- [3] S. Zhang, Y. An, X. M. Chen, I. Aprahamian, Q. Li, Responsive Mater. 2023, 1, 20230023.
- [4] Y. Q. Tang, X. Wang, S. L. Chen, Q. Li, Responsive Mater. 2024, 2, 20240003.
- [5] O. Ostroverkhova, Chem. Rev. 2016, 116, 13279.
- [6] D. Xiang, X. L. Wang, C. C. Jia, T. Lee, X. F. Guo, Chem. Rev. 2016, 116, 4318
- [7] Y. Xia, S. Chen, X. L. Ni, ACS Appl. Mater. Interfaces 2018, 10, 13048.
- [8] M. Gao, F. B. Yu, C. J. Lv, J. Choo, L. X. Chen, Chem. Soc. Rev. 2017, 46, 2237.
- [9] Q. Y. Liao, A. S. Li, A. R. Huang, J. Q. Wang, K. Chang, H. H. Li, P. F. Yao, C. Zhong, P. D. Xie, J. F. Wang, Z. Li, Q. Q. Li, *Chem. Sci.* 2024, 15, 4364.
- [10] B. Engels, V. Engel, Phys. Chem. Chem. Phys. 2017, 19, 12604.
- [11] R. F. Fink, J. Seibt, V. Engel, M. Renz, M. Kaupp, S. Lochbrunner, H. M. Zhao, J. Pfister, F. Wu"rthner, B. Engels, J. Am. Chem. Soc. 2008, 130, 12858.
- [12] Y. Hong, J. W. Y. Lam, B. Z. Tang, Chem. Soc. Rev. 2011, 40, 5361.
- [13] J. D. Luo, Z. L. Xie, J. W. Y. Lam, L. Cheng, H. Y. Chen, C. F. Qiu, H. S. Kwok, X. W. Zhan, Y. Q. Liu, D. B. Zhu, B. Z. Tang, *Chem. Commun.* 2001, 1740.
- [14] Y. Q. Tang, D. Xiang, Q. Li, Adv. Mater. 2025, 2501184.
- [15] S. Zhang, Y. An, X. M. Chen, Q. Li, Smart Mol. 2023, 1, 20230015.
- [16] U. Rösch, S. Yao, R. Wortmann, F. Würthner, Angew. Chem., Int. Ed. 2006, 118, 7184.
- [17] W. J. Newsome, A. Chakraborty, R. T. Ly, G. S. Pour, D. C. Fairchild, A. J. Morris, F. J. Uribe-Romo, *Chem. Sci.* **2020**, *11*, 4391.
- [18] Y. H. Ko, E. Kim, I. Hwang, K. Kim, Chem. Commun. 2007, 1305.
- [19] A. McLean, R. L. Sala, B. W. Longbottom, A. R. Carr, J. A. McCune, S. F. Lee, O. A. Scherman, J. Am. Chem. Soc. 2024, 146, 12877.
- [20] G. L. Wu, Z. H. Huang, O. A. Scherman, Angew. Chem., Int. Ed. 2020, 59, 15963.
- [21] S. Zhang, L. Y. Zhang, A. C. Chen, Y. An, X. M. Chen, H. Yang, Q. Li, Angew. Chem., Int. Ed. 2024, 63, 202410130.
- [22] B. H. Tang, W. Q. Xu, J. F. Xu, X. Zhang, Angew. Chem., Int. Ed. 2021, 133, 9470.
- [23] Y. Li, Z. Z Huang, A. X. Shao, Z. Q. Wu, Z. Y. He, H. Tian, X. Ma, Chem. Sci. 2025, 16, 6290.
- [24] Y. Li, Z. Q. Wu, Z. Z. Huang, C. J. Yin, H. Tian, X. Ma, Natl. Sci. Rev. 2025, 12, nwae383.

21951071, 2025, 29, Downloaded from https

onlinelibrary.wiley.com/doi/10.1002/adom.202501470 by Nankai University, Wiley Online Library on [26/10/2025]. See the Term:

of use; OA articles

are

governed by the applicable Creative Commons

www.advancedsciencenews.com

www.advopticalmat.de

- [25] G. L. Wu, Y. J. Bae, M. Olesi´nska, D. Antón-Garciá, I. Szabó, E. Rosta, M. R. Wasielewski, O. A. Scherman, *Chem. Sci.* 2020, 11, 812.
- [26] H. Yu, J. L. Li, S. S. Li, Y. Liu, N. E. Jackson, J. S. Moore, C. M. Schroeder, J. Am. Chem. Soc. 2022, 144, 3162.
- [27] X. L. Zhou, X. Bai, F. J. Shang, H. Y. Zhang, L. H. Wang, X. F. Xu, Y. Liu, Nat. Commun. 2024, 15, 4787.
- [28] H. J. Yu, Q. Y. Zhou, X. Y. Dai, F. F. Shen, Y. M. Zhang, X. F. Xu, Y. Liu, J. Am. Chem. Soc. 2021, 143, 13887.
- [29] X. K. Ma, W. Zhang, Z. X. Liu, H. Y. Zhang, B. Zhang, Y. Liu, Adv. Mater. 2021, 33, 2007476.
- [30] a) X. K. Ma, X. Zhou, J. Wu, F. F. Shen, Y. Liu, Adv. Sci. 2022, 9, 2201182. b) C. J. Yin, Z. A. Yan, R. J. Yan, C. Xu, B. B. Ding, Y. H. Ji, X. Ma, Adv. Funct. Mater. 2024, 34, 202316008.
- [31] H. J. Wang, W. W. Xing, H. Y. Zhang, W. W. Xu, Y. Liu, Adv. Opt. Mater. 2022, 10, 2201178.
- [32] Y. L. Wu, J. W. Zhou, B. T. Phelan, C. M. Mauck, J. F. Stoddart, R. M. Young, M. R Wasielewski, J. Am. Chem. Soc. 2017, 139, 14265.
- [33] X. R. Yang, S. M. Liu, Dyes Pigm. 2018, 159, 331.
- [34] D. F. Li, J. Wang, X. Ma, Adv. Opt. Mater. 2018, 6, 1800273.
- [35] Q. W. Zhang, D. F. Li, X. Li, P. B. White, J. Mecinovic', X. Ma, H. Ågren, R. J. M. Nolte, H. Tian, J. Am. Chem. Soc. 2016, 138, 13541.

- [36] G. T. Fan, X. Yu, X. Han, Z. Y. Zhao, S. M. Liu, Org. Lett. 2021, 23, 6633.
- [37] H. Wu, Y. Chen, X. Y. Dai, P. Y. Li, J. F. Stoddart, Y. Liu, J. Am. Chem. Soc. 2019, 141, 6583.
- [38] X. L. Ni, S. Y. Chen, Y. P. Yang, Z. Tao, J. Am. Chem. Soc. 2016, 138, 6177.
- [39] G. L. Wu, M. Olesińska, Y. C. Wu, D. Matak-Vinkovic, O. A. Scherman, J. Am. Chem. Soc. 2017, 139, 3202.
- [40] J. Wang, Z. Z. Huang, X. Ma, H. Tian, Angew. Chem., Int. Ed. 2020, 59, 9928.
- [41] K. N. Houk, A. G. Leach, S. P. Kim, X. Y. Zhang, Angew. Chem., Int. Ed. 2003, 42, 4872.
- [42] W. L. Mock, N. Y. Shih, J. Org. Chem. 1986, 51, 4440.
- [43] J. Lagona, P. Mukhopadhyay, S. Chakrabarti, L. Isaacs, Angew. Chem., Int. Ed. 2005, 44, 4844.
- [44] F. Biedermann, M. Vendruscolo, O. A. Scherman, A. De Simone, W. M. Nau, J. Am. Chem. Soc. 2013, 135, 14879.
- [45] F. Biedermann, V. D. Uzunova, O. A. Scherman, W. M. Nau, A. De Simone, J. Am. Chem. Soc. 2012, 134, 15318.
- [46] Deposition numbers 2417347 (for m-BPy), 2417351 (for p-BPy) contain the supplementary crystallographic data for this paper. These data are provided free of charge by the joint Cambridge Crystallographic Data Centre and Fachinformationszentrum Karlsruhe Access Structures service.